JOURNAL OF MECHANICAL ENGINEERING AND SCIENCES
ISSN: 2289-4659 e-ISSN: 2231-8380
VOLUME 18, ISSUE 4, 2024, 10261 - 10278
DOI: https://doi.org/10.15282/jmes.18.4.2024.4.0810

UNIVERSITI MALAYSIA PAHANG AL-SULTAN ABDULLAH

RESEARCH ARTICLE

Static and dynamic analysis of different MYSat frame structure

A. S. Mohamed Thaheer[1,2], N. A. Ismail[2]*, M. H. H. Amir[2], N. Abdul Razak[2]

[1] Faculty of Science, Hokkaido University, 060-0810 Sapporo, Hokkaido, Japan
[2] School of Aerospace Engineering, Universiti Sains Malaysia, Engineering Campus, 14300 Nibong Tebal, Seberang Perai Selatan, Pulau Pinang, Malaysia
Phone: +6045995944, Fax.: +6045996911

ABSTRACT – The development of CubeSats have been advanced following the miniaturization of electronic components. While CubeSats have been extensively used in various missions, most prior research has focused on validating their structural design to comply with deployer requirements. Thus leaving a gap in understanding the structural performance of different CubeSat frame configurations. This study analyzes two MYSat CubeSat frame designs, modular and monoblock and was conducted using the ANSYS Mechanical package to assess and compare the mechanical properties of each design. The results showed that the modular frame exhibited greater deformation of 4.4×10^{-7} m and a von Mises stress of 0.74 MPa in the stowed configuration compared to the monoblock. During launch, the modular frame displayed higher deformation and stress under Orbital Cygnus launcher conditions, with natural frequencies of 679.99 Hz and 677.88 Hz for the modular and monoblock frames, respectively. Under PSLV launch conditions, peak stresses were 12.70 MPa for the modular frame and 16.39 MPa for the monoblock frame during random vibration analysis. Stress concentrations were primarily observed at standoffs supporting circuit boards, posing potential risks of loosening or damage. Despite these findings, both designs remained within the Al-6061 yield strength, ensuring structural integrity. This research highlights the importance of evaluating different CubeSat configurations to optimize their design for better resilience under launch stresses. It suggests further analysis incorporating larger satellite components to enhance the accuracy of structural performance assessments.

ARTICLE HISTORY
Received : 09th May 2024
Revised : 18th Nov. 2024
Accepted : 22nd Nov. 2024
Published : 30th Dec. 2024

KEYWORDS
Cubesat
Structural analysis
Frame design
Static analysis
Modal
Random vibration

1. INTRODUCTION

Rapid advancements in miniaturization and integration of electronic components have played a crucial role in developing small satellites [1]. When CubeSats were first introduced through a collaboration between Stanford University and California Polytechnic State University via the Poly Picosatellite Orbital Deployer, it became a cornerstone of affordable space research. The NanoRacks CubeSat Deployer and the current Japanese Experimental Module Small Satellite Orbital Deployer (J-SSOD) onboard the International Space Station (ISS) have become the gold standard for its deployment. The design of these deployers significantly affects the mechanical requirements of CubeSat subsystems. As a result, the Universiti Sains Malaysia Space Systems Laboratory initiated the MYSat CubeSat project to measure electron density in the Ionosphere E-layer [2]. Designed as a 10 cm × 10 cm × 10 cm CubeSat weighing approximately 1 kg, the MYSat has a temperature and electron density probe as its primary payload. It is expected to maintain a circular orbit at 380–420 km altitude, mirroring the ISS [3]. Standard 1-unit CubeSats typically have a mass of 1.33 kg and a volume of 10 cm^3, utilizing integrated circuit modules that adhere to established standards. This standardization facilitates compatibility among the developers. Although the project's scientific goals are well established, the mechanical design of the CubeSat structure remains a critical aspect of the mission, given the need to withstand the harsh dynamic loads of launch and space environments. For the success of these and other CubeSat projects, optimization of CubeSat structures to balance strength, durability, and minimum weight while ensuring reconfiguration for future missions is essential.

Cote et al. [4] and Raviprasad et al. [5] have identified four primary structural configurations for CubeSat design: monoblock, double monoblock, panel-based, and modular frames. Monoblock designs are characterized by their simplicity, lightweight, and rigidity, which enhance their overall structural strength. This approach also avoids the concentrated stresses associated with fasteners during assembly, providing proper alignment and support for the structural components. Examples of CubeSats utilizing the monoblock concept include the SwissCube and the SATAX Project. However, this design may present challenges in terms of accessibility and troubleshooting, as the primary structure cannot be easily removed, unlike in the modular approach. In addition, the manufacturing process for monoblock designs can result in excessive waste and residual internal stresses, as observed in the EquiSat Brown Space Engineering project. In contrast, modular frame design, exemplified by FITSAT-1, offers greater flexibility for the development and integration of subsystems and payloads. This approach is generally easier to fabricate using smaller individual metal blocks and results in fewer residual stresses during assembly. Nevertheless, modular frame design faces difficulties in achieving the

*CORRESPONDING AUTHOR | N. A. Ismail | ✉ aenorilmi@usm.my

required external geometrical tolerances, and bolted joints can increase the overall mass and introduce concentrated stresses.

Previous studies have focused mainly on confirming the structural designs and conducting analyses to ensure that CubeSat structures meet the requirements set by deployers. Various researchers have examined either monoblock [6-9] or modular [5, 10-20] frame designs and evaluated their performance through static, dynamic, modal, and random vibration analyses. These studies generally produced results within specified limits, whereas structural design optimisation is recognized as an essential consideration. The work in [21] explored beam-on-rail configurations but only considered static loading, concluding that there is no single "best" CubeSat structure design; rather, the most suitable design depends on the specific mission profile. Other researchers, such as [28] and [29], have compared the performance of different materials in their structural designs. State author name [28] found that Carbon-fibre Reinforced Polymer (CFRP) composites offer a better strength-to-weight ratio than Aluminium 7075-T6 and carbon-epoxy T300-5208, whereas Garg et al. [29] selected Aluminium 7075-T6 due to its higher stiffness.

Although CubeSats have been widely adopted for various space missions, there remains a critical need for in-depth research on the structural performance and behaviour of different CubeSat frame designs, particularly their ability to withstand launch-induced stress and deformation. Mechanical failures during launch stemming from excessive deformation or structural stresses can jeopardize mission success, underscoring the importance of optimized structural designs that can endure launch conditions without compromising functionality. This research investigates explicitly the mechanical design and finite element analysis of two structural configurations of the MYSat CubeSat: modular and monoblock frames. This study aims to develop a structurally optimized CubeSat design that minimizes mass while maintaining mechanical integrity, determines the maximum deformation amplitude within acceptable limits for the specified minimum natural frequency, and conducts a random vibration analysis to evaluate load stresses under simulated launch conditions. Furthermore, this research proposes a lightweight CubeSat configuration capable of withstanding anticipated mechanical loads while offering flexibility for reconfiguration in future missions. These objectives align with the broader goal of advancing CubeSat structural design to ensure durability, adaptability, and mission success in the rapidly evolving field of space technology.

2. MATERIAL AND METHODS

2.1 Design Concept

The primary requirements for subsystem structures are to provide interfaces for each subsystem and accommodate multiple payloads while adhering to the design constraints [20]. The structure consists of three main components: rails, beams, and panels, which form the four fundamental frame designs [4, 5]. The four edges of the MYSat were formed by rails and beams, and the MYSat launch interfaces determined its dimensions. Brackets and fasteners were used to attach the internal components of the structure. The choice of the main chassis significantly affects the arrangement of the internal components and the material selection for the satellite structure. According to Sandau et al. [24], there are three methods for arranging circuit boards within a CubeSat: stacking, slotting, and placement on the sides. Stacking is commonly employed because it offers robust rigidity to the CubeSat by placing all subsystems in a stacked configuration, forming a secondary structure. However, this secondary structure adds extra mass to the system, and it can be challenging to establish connections and route cables between nonadjacent subsystems.

As outlined in [25, 26], the satellite structure design process is iterative. The design requirements were carefully examined at each stage to ensure their fulfilment. If any requirements remain unmet, the design and analysis are iteratively refined until the desired objectives are achieved. The satellite launch and deployment requirements are determined based on the quasi-static launch loads and the natural frequencies of the launcher and deployer. The primary structural components of the satellite were analysed using Analysis Systems (ANSYS) V15 Workbench (ANSYS, Inc., Canonsburg, PA, USA). Commonly available launch vehicles, such as the H-II Transfer Vehicle (HTV), Automated Transfer Vehicle (ATV), SpaceX Dragon, Orbital Cygnus, and Polar Satellite Launch Vehicle (PSLV), were utilized, and deployment was facilitated using the J-SSOD module. The satellite specifications detailed in the Japanese Experiment Module (JEM) handbook must strictly adhere to [27]. Thaheer et al. [2] describe these specifications and operational concepts, imposing constraints and requirements on the satellite design, ensuring compatibility with the interface adaptor, and enabling seamless integration and functionality.

In addition to the abovementioned requirements, the satellite structure subsystem must fulfil several criteria. These include providing suitable mechanical interfaces and housing to securely hold various satellite components and subsystems, enabling proper integration and functioning. The structure must also be designed to withstand harsh space environments, including exposure to radiation and mechanical stresses during launch, deployment, and operation. Furthermore, the structure must adhere to the specific requirements of the selected deployer or launcher to ensure compatibility and successful satellite deployment. The structure should incorporate a system to organize and route electrical harnesses, ensuring proper connectivity between different components and subsystems. Additionally, the structure should be designed to maximize strength while minimizing weight, as this strength-to-weight ratio is critical for achieving an optimal balance between the structural integrity and overall satellite mass. By addressing these supplementary requirements, the satellite structure subsystem can contribute to overall mission success by providing mechanical stability, protection, and efficient integration of various satellite components.

2.1.1 Computer-aided design

The computer-aided design (CAD) structure and components of MYSat were modelled using Computer-Aided Three-Dimensional Interactive Application (CATIA) V5R21 (Dassault Systèmes, Paris, France) software. The design of the MYSat structure was based on the Innovative Solutions in Space 1U CubeSat structure, which was selected because of its availability as an experimental unit in the laboratory and its proven flight heritage. The modular design of the Innovative Solutions In Space (ISISPACE) (ISISpace Group, Delft, Netherlands) CubeSat structure provides convenient access for troubleshooting and can accommodate multiple printed circuit board sizes. Additionally, it incorporates a dual-kill-switch mechanism [28]. The original ISISPACE CubeSat structural design was modified to satisfy the specific requirements of the MYSat mission. Furthermore, a monoblock structure was designed using different board-mounting methods for a comparative analysis. Figure 1(a) shows the MYSat assembly design using a modular frame.

The MYSat structure adheres to the cube primary frame structure guidelines specified in the JEM handbook [27]. The secondary structure of MYSat consists of four electronic boards positioned flexibly within the satellite. Figure 1(b) illustrates the arrangement of these components. The temperature and electron density probe (TeNeP) science unit is at the top of MYSat, whereas the antenna deployment system is at the bottom. The solar panels cover all four sides of MYSat, and the electrical power and communication systems are strategically placed in the lower section, away from the centre of gravity, to ensure attitude stability using a gravity gradient. A 20 mm brass standoff separates the power system from the communication system. The onboard computer was positioned at the third level, followed by the TeNeP system at the fourth level. Furthermore, brass standoffs connect all circuit boards to the primary structure.

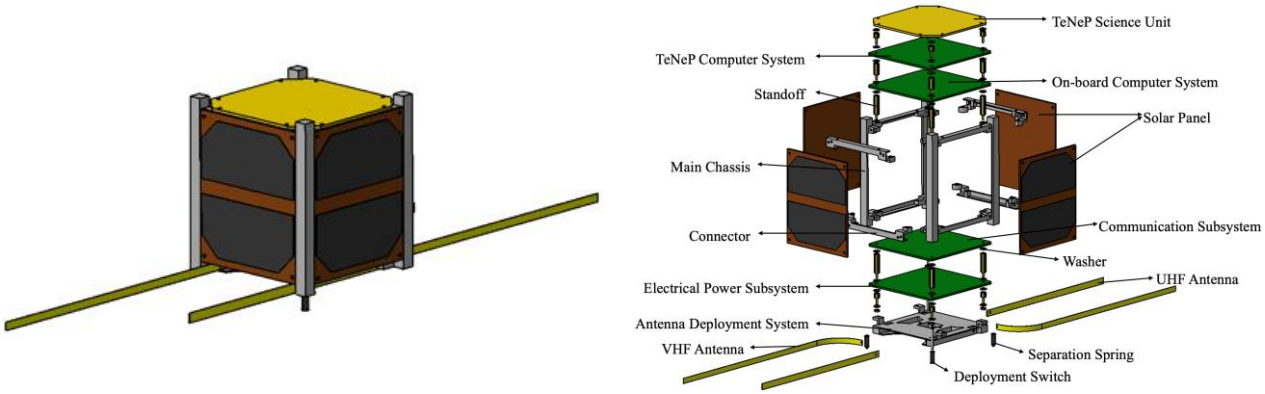

(a) (b)

Figure 1. MYSat design: (a) Assembly design and (b) Exploded view of MYSat

Figure 2 illustrates the initial conceptual design of the MYSat frame, showing both the monoblock and modular frame configurations. The modular frame comprises two interconnected square-ring structures facilitated by four connectors. Conversely, the monoblock frame presents a singular solid body while preserving the same characteristics as in the modular design. The monoblock structure eliminates the need for connectors and reduces reliance on joints. This design decision also influences the placement of the internal boards, as depicted. This deliberate approach enables a comparative structural analysis of the two designs and evaluates their respective performance.

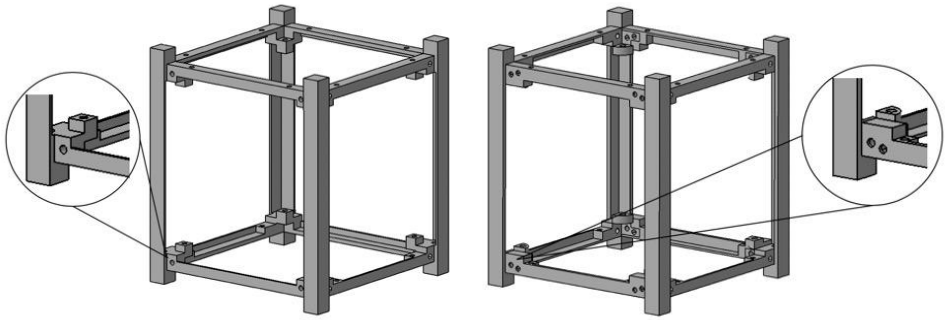

(a) (b)

Figure 2. Preliminary MYSat frame design concept: (a) Modular frame and (b) Monoblock frame

2.1.2 Material selection

The selection of materials is critical in satellite design because high-density materials can increase the structural weight, impact orbital performance, and reduce the available space for other components. Factors such as manufacturability, cost, and mechanical and thermal properties must also be considered [29]. The ITÜpSAT II satellite [16] and the analysis performed by Israr [30] revealed that Aluminium 7075 was chosen for its manufacturability and high stiffness despite its higher weight compared to Aluminium 6061 [8, 25, 31]. Similarly, Aluminium 2024-T3 was selected in [7] because of the local unavailability of Aluminium 6061 and Aluminium 7075, although the chosen materials

had similar properties. For the CUTE-1 satellite, a magnesium alloy was used as the structural member to achieve a lightweight design [32]. Additionally, a space-approved composite material, HTM143/M55J Cyanate-Ester/Carbon unidirectional prepreg made by CYTEC, was utilized, providing a significant advantage in terms of strength-to-weight ratio, resulting in a mass reduction of nearly 40% [33]. However, materials other than those listed by the Japan Aerospace Exploration Agency require flammability and outgassing tests for safety verification, which can increase project costs.

This study aims to design a structural framework for the MYSat satellite that exhibits a high strength-to-weight ratio, is cost-effective, and can be easily manufactured and maintained. After thoroughly evaluating the mechanical and thermal properties, manufacturability, cost, and availability, Aluminium 6061-T6 was selected as the material for the MYSat structure. This decision was based on the material's advantageous combination of properties, which enabled it to meet project requirements. Furthermore, Aluminium 6061-T6 can withstand extreme thermal cycling that may occur during satellite deployment. 1 lists the material properties of the MYSat structure and its components. The baseline design of MYSat is still under development because of its internal components. Consequently, this study focused solely on circuit board placement and material properties within the MYSat structure, excluding the electronic components of the PCBs.

1. Summary of MYSat material properties

Properties	Al6061-T6 [34]	AISI 304 Stainless Steel [35]	Brass [36]	FR4 PC/104 [37]
Density (kg/m^3)	2700	8000	8490	2200
Ultimate Tensile Strength (MPa)	310	505	338	428
Young's Modulus (GPa)	68.9	197	97	20
Poisson's Ratio	0.33	0.29	0.31	0.30
Component Assignment	MYSat frame TeNeP plate Antenna Deployment Solar Panel	Washer	Standoff	PCB

*Al: Aluminium; AISI: American Iron and Steel Institute; FR: Flame Retardant

2.1.3 MYSat mechanical properties

Ensuring that MYSat remains within the specified weight limit of 1.33 kg is crucial and requires regular monitoring and updates regarding the satellite's mass throughout the project. Given that the components of MYSat are yet to be finalized, there can be significant variations in the mass budget. A careful mass trade-off was conducted to address this challenge, considering the available 1U CubeSats and relevant literature. The satellite's total mass is used to calculate the average mass percentage of each subsystem. However, it is essential to note that certain assumptions were made during the analysis. First, the payload mass is mission-specific. Second, specific estimations were made based on limited detailed information in the literature. Third, the solar panel mass in the power system was accounted for. Finally, any mechanisms present are considered part of the overall structure. These assumptions aid in comprehensively analysing the satellite mass distribution and its subsystems. According to the data presented in Table 2, the payload, power, and structural subsystems account for a significant portion of the total mass, surpassing the mass contributions of other subsystems. Although thermal control is not typically incorporated in a 1U CubeSat, thorough thermal analysis and strategic component placement are essential to prevent potential thermal issues. Additionally, miscellaneous components, such as cabling, electronic components, screws, and adhesives, are considered less well-researched in the literature. However, it is worth noting that the average total mass of the satellite, when compared to a previous CubeSat and lightweight satellite, remained below the mass requirement set by the JEM.

Table 2. The mass budget trade-off between 1U CubeSat examples and lightweight satellites [38-40]

Subsystems	NPS-SCAT	ArduSat-1	SMAD	Average
Payload	15.51%	8.00%	24.40%	15.97%
Structure	16.10%	10.77%	22.70%	16.52%
OBDH	11.02%	5.50%	6.70%	7.74%
ADCS	0.01%	0.01%	11.30%	3.77%
Thermal	0.00%	0.00%	0.00%	0.00%
Communication	0.08%	2.45%	6.00%	2.84%
Power	36.00%	42.80%	24.60%	34.47%
Misc.	12.49%	30.47%	4.30%	15.75%
Total (kg)	0.93	1.00	1.33	1.09

*OBDH: On-board Data Handling; ADCS: Attitude Determination and Control System; Misc.: Miscellaneous

Table 3 presents the evaluation of the mass of the proposed CAD design using CATIA Inertia tools. The two designs, excluding the complete components, weighed 596 g and 617 g for modular and monoblock, respectively. The results balance approximately 50% of the total mass required to complete the design. When comparing the mass distribution of the subsystems in Table 3 with the data in Table 2, it can be observed that the masses of all the subsystems are relatively similar, resulting in a maximum total mass of 1.33 kg. This mass budget provides valuable insights into the limitations and considerations of developing and procuring MYSat subsystems.

Table 3. Evaluated masses from CATIA software

Subsystems	Modular	Monoblock	Average (Table 2)
	Weight (kg)	Weight (kg)	Weight (kg)
Payload	0.234	0.234	0.212
Structure	0.139	0.118	0.220
OBDH	0.034	0.034	0.103
ADCS	-	-	0.050
Thermal	-	-	0.000
Communication	0.034	0.034	0.038
Power	0.234	0.234	0.458
Antenna Deployment	0.059	0.059	N/A
Misc.	-	-	0.209
Total (kg)	0.734	0.713	1.330
Requirement (kg)	1.330	1.330	1.330
Margin (kg)	0.596	0.617	0.000

Furthermore, according to JEM, it is essential to ensure that the centre of gravity (COG) of the 1U MYSat remains within a 20 mm radius from its geometric centre. This requirement emphasizes the significance of accurately modelling the subsystems' mass distribution and the satellite's internal structure. The CATIA Inertia tool was utilized in the assembly configuration to determine the COG position. The magnitude of the COG was calculated using Eq. (1) to validate its compliance with the 20 mm sphere constraint.

$$d = \sqrt{x_{COG}^2 + y_{COG}^2 + z_{COG}^2} \tag{1}$$

where d is the magnitude of the COG position vector and x_{COG}, y_{COG}, and z_{COG} are the COG coordinates. The COG coordinates were determined using CATIA Inertia tools and are presented in Table 4. These values demonstrate that the mass distribution within the satellite is uniform, falling within the specified 20 mm range as required by the Japan Aerospace Exploration Agency (JAXA). However, it is essential to note that COG and inertia measurements should be experimentally verified once a complete satellite is available. Experimental verification will provide a more accurate assessment of the COG and inertia characteristics, ensuring that they align with the calculated values and further validating the structural integrity of the satellite.

Table 4. MYSat centre of gravity coordinates for both designs

Axes	Coordinates (mm)	
	Modular	Monoblock
X	0.000	0.000
Y	0.000	0.000
Z	−0.850	−1.015
d	0.850	1.015

The JEM specifies that a stowed satellite's Ballistic Number, BN, should not exceed 100 kg/m^2 for a faster orbiting decay of the satellite than the ISS. Nogawa et al. [41] stated that BN can be expressed mathematically using Eq. (2).

$$BN = \frac{m}{C_D A}, \tag{2}$$

where the average drag coefficient, C_D, for the 1U CubeSat is 2.2, and A is the reference area of the MYSat, which can be estimated using Eq. (3), as proposed in [42].

$$A = H \sin(\alpha) + W \cos(\alpha), \tag{3}$$

where H is the satellite height, W is the satellite width, and α is the satellite angle of attack. Estimating each angle of attack from +90° to -90° indicates that α = 49° produces the maximum frontal area. The ballistic number for MYSat was determined to be 4 kg/m², which was below the limit set by the JAXA requirement of 100 kg/m².

Finally, the margin of safety (MOS) was employed to assess the structural safety of the system. The MOS is determined by the ratio of allowable load to applied load, as shown in Eq. (4). Typically, the FR4 PC/104 material used for PCB has a safety factor (SF) 1.4. However, a safety factor of 2 was assumed and multiplied by the applied load for simplicity. This approach ensures a conservative estimate of the safety margin, and enhances the structural integrity of the system.

$$MOS = \frac{Load_{Allow}}{Load_{Applied} \times SF} - 1 \tag{4}$$

where, $Load_{Allow}$ is the allowable load, $Load_{Applied}$ is the applied load, and SF is the safety factor. Table 5 provides an overview of the safety margin for the modular and monoblock frame designs under maximum applied load. Both designs demonstrated a positive margin of safety due to the high allowable strength of the materials used. However, it is important to note that this calculation did not consider the presence of complete MYSat components. Larger components, such as batteries and communication boards, can impose additional stress on the material, potentially reducing the safety margin. Therefore, it is crucial to consider the requirements and stresses induced by a complete set of components to ensure an accurate assessment of the safety margin for the chosen frame design.

Table 5. MYSat concept design margin of safety

Parameter	Design	
	Modular	Monoblock
Margin of Safety	7.89	8.46

2.2 Finite Element Modelling

Structural analysis was performed using the ANSYS Mechanical package in the ANSYS software. The assembly of all the components in the design allowed for a comprehensive examination of the entire structure. This process identifies weaknesses in the MYSat structure, highlighting areas that require further improvement. The contacts between the joints were appropriately defined to ensure uniform load distribution across the body. In addition, tetrahedral mesh elements of appropriate sizes were employed throughout the structure, as shown in Figure 3. This choice of element shape is supported by previous studies [25, 43], demonstrating its ability to model complex shapes accurately. The ANSYS analysis settings are listed in Table 6.

Figure 3. MYSat meshing configuration in ANSYS

Table 6. Summary of ANSYS analysis setup

Parameters	Remarks
Contacts	All contacts are merged
Mesh Method	Tetrahedrons: Patch Conforming
Sizing	Relevance Centre: Fine
	Element Size: Default
	Smoothing: Medium
	Transition: Fast
	Span Angle Centre: Medium
Statistics	Nodes: 205805
	Elements: 101335

2.2.1 Loading, boundary and initial conditions

The satellite is subjected to various mechanical loads throughout its life cycle, particularly during the launch phase, which involves high loads [21]. A comprehensive analysis was conducted to ensure the survival of MYSat during launch and its safe deployment from the launch vehicle. This type of analysis includes static, modal, and random vibration analyses [8, 19, 25]. The applied load assumes a worst-case scenario in which MYSat is at the lowest vertical position, as described in [7]. Mahesh et al. [44] also account for lateral loads acting concurrently with longitudinal loads, including the effects of Earth's gravity applied to the centre of gravity of the CubeSat as body forces. For static analysis, the total force in this case was divided by four to determine the individual load on each MYSat leg. Furthermore, Raviprasad and Nayak [5] specified that the four legs at the bottom of the CubeSat are fixed and aligned in the direction of lateral forces. Based on [30], it was assumed that the site launch vehicle constrained the satellite analysis; bolted joints were disregarded because of their small dimensions. However, if bolted screw joints are considered, an empirical calculation of bolt pretension can be performed according to the guidelines outlined in [45]. This method increases the complexity of the analysis because many bolted joints exist in the design. Alternatively, Raviprasad and Nayak [5] simplified the computations by treating tertiary components, including payloads and bolted joints, as point masses positioned at the centre of gravity of each element. The MYSat analysis selected the joint area as bonded in ANSYS contact settings to simulate bolted attachments. Regarding load factor calculation, while the National Aeronautics and Space Administration's (NASA) General Environmental Verification Standard [46] is commonly referenced, Raviprasad and Nayak [5] assumed a value of 1.5 for each inertial load in their analysis.

The boundary conditions were defined by fixing the satellite's legs at their base to prevent rigid-body motion during static and quasi-static analyses. This setup allowed the structure to react to applied forces while maintaining structural stability. In the dynamic analysis, the satellite was constrained to the bottom and aligned according to the coordinate system of the launch vehicle. For modal analysis, boundary conditions were imposed to prevent the satellite base's movement while allowing the upper structure's vibration. This approach ensured that the natural frequencies of the satellite remained within safe operational limits. For all the analyses, the initial conditions were presumed to be zero displacement and zero velocity, ensuring that the structure was in a state of rest before applying external loads. In the random vibration analysis, no residual stresses or pre-existing loads were considered, permitting the model to simulate the effects of vibration exclusively due to launch loads.

Upon completion of the mechanical load analysis, specific boundary conditions were applied and carefully chosen, considering the conditions MYSat may encounter during transport and deployment. It is essential to note that the orientation of the deployment system within the launch vehicle is a crucial factor that must be considered. The direction of the deployment system must be determined before the MYSat launch, and the MYSat design should be aligned with this requirement to ensure a successful deployment. In scenarios with uncertainty or ambiguity regarding MYSat orientation during launch, modelling and analysis should be conducted under the worst-case scenario assumption. This analysis should involve static, modal, and random vibration analyses to ensure that MYSat can withstand the forces and stresses encountered during the launch and deployment.

2.2.2 Static analysis

Static and quasi-static analyses were performed to estimate satellite structural components' stress, strain, and displacement. These analyses play a crucial role in assessing the satellite structure's strength and verifying the design load's safety margin. During the static structural analysis, a force is applied to the body under specific conditions. The study considers two key conditions: the equilibrium state and the rocket launch phase. Quiroz-Garfias et al. [19], a structure can withstand loading conditions if the measured values are lower than the specific material properties. MYSat is situated inside J-SSOD, along with two other satellites, during the equilibrium condition while awaiting launch clearance. MYSat was assumed to be positioned at the bottom of J-SSOD, denoted as position 3 in Figure 4(a), bearing the weight of the two satellites above it and the reaction force from the spring.

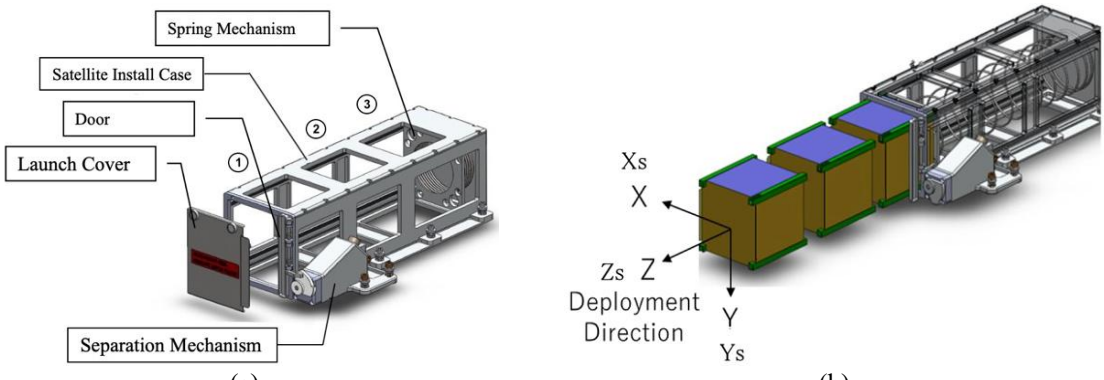

(a) (b)

Figure 4. J-SSOD: (a) External view of the deployer [47] and (b) Coordinate system definition. The Z-axis represents the launch direction [47]

However, incorporating this load into ANSYS is a challenging task. Initially, ANSYS reported an error related to detecting rigid-body motion, likely due to the system's absence of a fixed support or clamping. The analysis was performed under two conditions for both designs to address this issue, as summarized in Table 7. A free-body diagram visually depicting the system is shown in Figure 5.

Table 7. Case study for static analysis under equilibrium conditions

Static Case	Descriptions
1	Fixed support at the bottom
	The load is applied to the top using the weight of the two satellites
2	Fixed support at the top
	The load is applied at the bottom using the spring reaction force

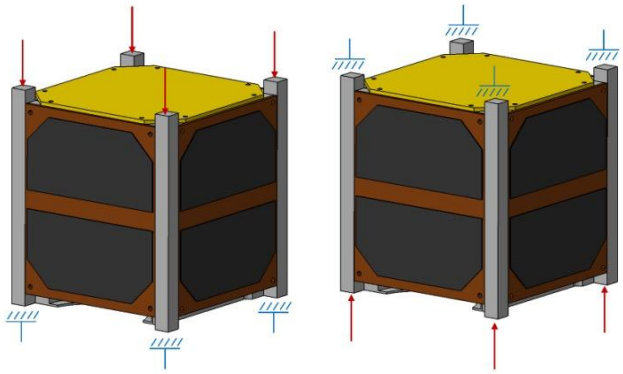

(a) (b)

Figure 5. The free-body diagram for static analysis (red arrow: direction of force; blue symbol: position of fixed support): (a) Static Case 1 and (b) Static Case 2

This configuration helps to identify study cases that represent the worst-case conditions. The load for Static Case 1 was calculated using Eq. (5). In contrast, the load for Static Case 2 is provided in the JEM handbook, which is 46.6 N, assuming the satellite has a maximum mass of 1.33 kg.

$$F = 2mg = 2(1.33)(-9.81)$$
$$F = -26.1\ N\ (-\text{ indicates opposite direction}) \quad (5)$$

where, m is the satellite mass in kg, and g is the gravitational acceleration in ms^{-2}. During the launch phase, a new gravity-like acceleration known as the G-load was introduced and applied to the centre of the geometric structure. Simultaneously, the lower legs of the base were fixed to facilitate the computation of quasi-static analysis. The previously applied force must be recalculated by using the new load factor derived from Eq. (6). The load factor values were obtained from the studies conducted by State Author name [27] and Ramakrishnan et al. [48], as outlined in Table 8. In the worst-case scenario, the load factor is assumed to be equal in all directions.

$$F = 3mng \quad (6)$$

where n is the load factor. The G-load was applied based on the coordinate frame designated in the JEM handbook, as illustrated in Figure 4(b).

Table 8. Maximum vehicle acceleration

Launcher	Load Factor (adimensional)	G-load (m/s^2)	New Applied Force (N)
HTV	8.34	81.78	326.11
ATV	12.37	121.30	483.99
SpX Dragon	8.67	85.02	339.22
Orbital Cygnus	18.10	177.49	708.18
PSLV	6.20	60.80	242.58

However, ANSYS cannot simultaneously model the G-load in all directions. ANSYS requires separate cases to calculate the G-load magnitude because the G-load is expressed as a vector. Three cases were considered to address this limitation, as outlined in Table 9. Each case represented a specific G-load direction, assuming the same applied load, thereby overcoming this issue.

Table 9. Launch case study for static analysis under launch conditions

Launch Case	G-load	Applied Force
1	+X	The direction of the force is unchanged
2	+Y	
3	+Z	

2.2.3 Dynamic analysis

The dynamic analysis focuses exclusively on modal and random vibrations. The modal analysis outcomes are directly linked to the initial setup and prerequisite data necessary for random vibration analysis. The analysis incorporated the relevant boundary conditions shown in Figure 6, which were applied based on the inertial load limitations of the launch vehicle. The objective of the modal analysis was to ensure compliance with the global stiffness requirements mandated by J-SSOD. The aim was to verify whether the minimum fundamental frequency of the entire system exceeded 100 Hz. This constraint prevents the resonance phenomena from occurring when the loading vibration frequencies coincide with the structure's natural frequencies. Such resonance phenomena pose significant challenges to dynamic structures [5], [49]. The dynamic characteristics of the structure under consideration depend primarily on its weight and stiffness.

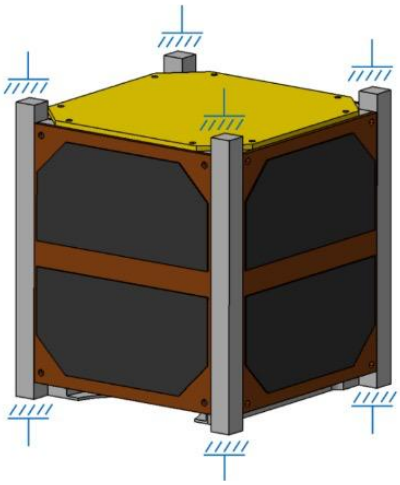

Figure 6. The free-body diagram for modal analysis

Contrastingly, random vibration analysis assesses the structural response to random dynamic loading conditions [30]. This analysis incorporates all launchers recommended by JAXA and includes a PSLV launcher from India. The study employed the power spectral density (PSD) spectrum provided by JEM and PSLV to represent the applied load. The relationship between PSD and frequency is depicted in Figure 7.

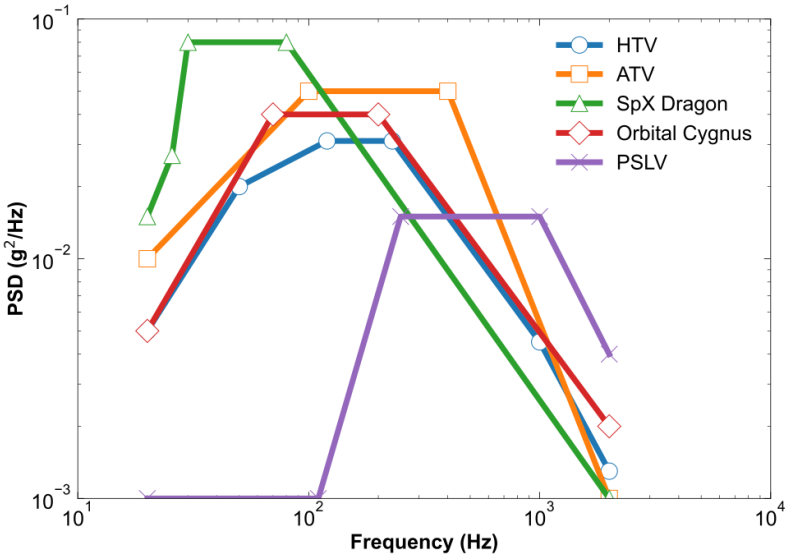

Figure 7. Random vibration of each available launch vehicle [27, 48]

3. RESULTS AND DISCUSSION

3.1 Static Analysis - Equilibrium

The static analysis of the modular and monoblock frame designs, as detailed in Section 0, examined two primary loading scenarios, as summarized in Table 7. In Static Case 1, a fixed support was applied at the bottom of the structure, with the load exerted from the top to represent the combined weight of the two satellites. In Static Case 2, a fixed support was applied at the top of the structure, while the load was used from the bottom to simulate the spring reaction force. Table 10 presents the total deformation and von Mises stress for both frame designs in each case. Generally, the deformations observed in both designs range from approximately 1.6 to 4.4 × 10^{-7} m, while the von Mises stress ranges from 0.24 to 0.74 MPa. Static Case 2 causes nearly twice large deformations and von Mises stress than Static Case 1, which is attributed to the larger load applied in Static Case 2, as calculated in Section 0. Figure 8 and Figure 9 depict the distribution of deformation in both the monoblock and modular frame designs for Static Cases 1 and 2, respectively. In Figure 8, the maximum deformation of Static Case 1 was observed at the top recessed feet of MYSat. In contrast, in Static Case 2, as observed in Figure 9, the maximum deformation was mainly at the bottom of the satellite. This behaviour was expected because both maximum points were located at the sites of the applied loads, as depicted in Figure 5.

Table 10. Comparison of static case analysis under equilibrium conditions for both designs

Static Case	Modular		Monoblock	
	Max. Total Deformation (× 10^{-7} m)	Max. von Mises Stress (MPa)	Max. Total Deformation (× 10^{-7} m)	Max. von Mises Stress (MPa)
1	2.701	0.444	1.560	0.235
2	4.420	0.744	2.850	0.417

The data in Table 10 reveal that the modular frame design exhibits a higher total deformation than the monoblock frame design under both loading scenarios. This finding can be attributed to the uniform load distribution and inherent resilience of the monoblock's unibody concept, which helps reduce deformations and stresses. Figure 10 and Figure 11 illustrate the von Mises stress distributions for the monoblock and modular frame designs for Static Cases 1 and 2, respectively. Figure 10(a) shows that the modular frame experiences stress at both the top and bottom recessed feet. In contrast, the maximum stress point for the monoblock frame in Figure 10(b) is caused by the bending of the top recessed feet. This behaviour may be due to the fixed support holding the satellite at the bottom-recessed feet of the modular frame, as shown in Figure 11. Additionally, Figure 11(b) suggests that the monoblock frame has a better structural strength because a larger load is required to cause the same stress behaviour, as shown in Figure 11(a).

The presence of holes in the design, as indicated in Table 10, can be associated with increased total deformation and stress of the structure. These holes create stress concentrations in the surrounding areas, rendering the structure more susceptible to failure, as discussed in the literature [12, 50]. Stress concentrations occur because of the localized redistribution of stress around the hole edges, leading to higher stresses in these regions. This observation aligns with previous findings [20], which reported the maximum stress occurring at the screw holes and the highest total displacement at the frame feet. Therefore, careful consideration should be given to the design and placement of holes in the structure to minimize stress concentrations and ensure the satellite's overall structural integrity and performance. Overall, the results indicate that the modular and monoblock frame designs exhibit excellent structural stability with deformations within the specifications for Al-6061, which has a yield strength of 310 MPa for the given loading and boundary conditions. This suggests that the selected material can effectively withstand applied loads without exceeding its stress limit [5].

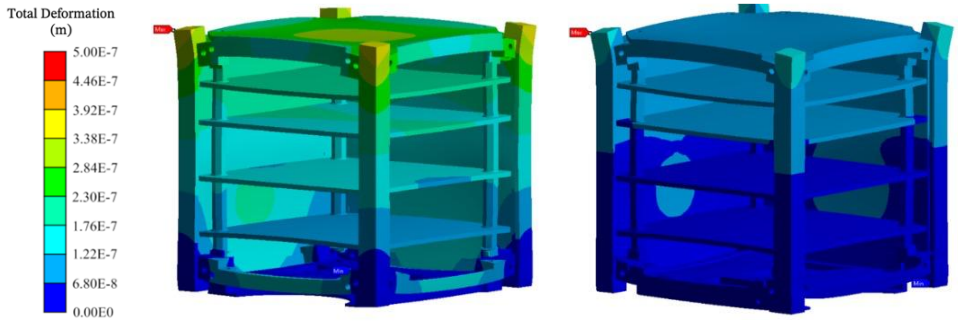

(a) (b)

Figure 8. Total deformation for Static Case 1: (a) Modular frame and (b) Monoblock frame

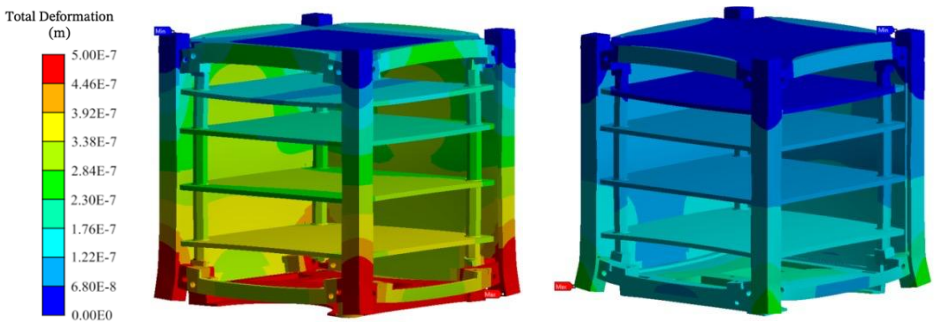

(a) (b)

Figure 9. Total deformation for Static Case 2: (a) Modular frame and (b) Monoblock frame

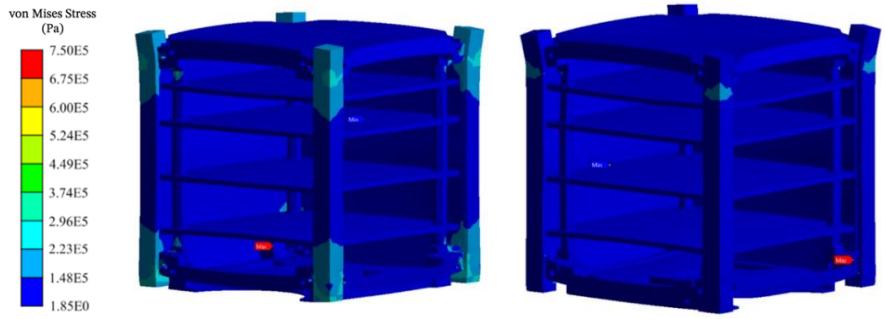

(a) (b)

Figure 10. von Mises stress for Static Case 1: (a) Modular frame and (b) Monoblock frame

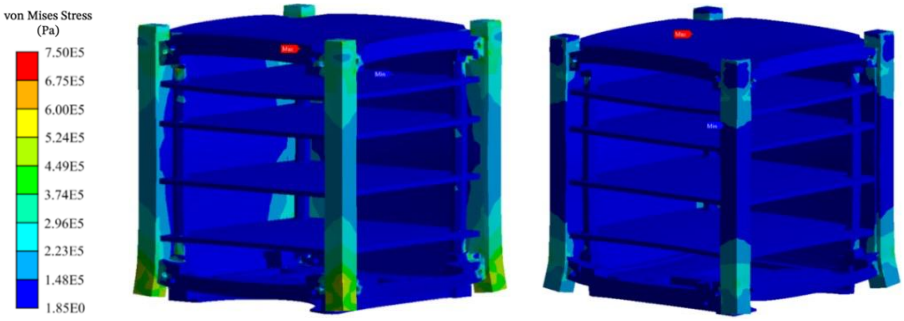

(a) (b)

Figure 11. von Mises stress for Static Case 2: (a) Modular frame and (b) Monoblock frame

3.2 Static Analysis - Launch

The static analysis examined the structural performance of the modular and monoblock frames under various launch vehicle conditions, and the results are presented in Table 11. The tables compare the maximum total deformation and von Mises stress along both frame designs' X-, Y-, and Z-axes. The modular frame generally exhibited higher stress and deformation than the monoblock frame across all launch scenarios, suggesting that the monoblock design may offer greater structural robustness under launch loads.

For the modular frame, the highest total deformation occurred with the Orbital Cygnus launcher, reaching 20.11×10^{-6} m along the X-axis. In contrast, the lowest deformation was observed with the PSLV at 6.89×10^{-6} m in the same direction. Similarly, the monoblock frame experienced the greatest deformation with the Orbital Cygnus launcher, showing a maximum of 18.20×10^{-6} m along the X-axis, and the lowest deformation was also observed with the PSLV at 6.24×10^{-6} m. The largest deformations were observed at the top PCBs of both frame designs during the launch scenarios, as shown in Figure 12. However, these displacements remained relatively small and were considered negligible, with no significant effect on the structural integrity or performance of the frames.

Table 11. Comparison of static analysis during launch conditions for both designs for different launch vehicles: (a) Modular frame and (b) Monoblock frame

Launcher	(a) Modular Frame					
	Max. Total Deformation ($\times 10^{-6}$ m)			Max. von Mises Stress (MPa)		
	X	Y	Z	X	Y	Z
HTV	9.27	4.14	3.83	5.78	7.80	8.03
ATV	13.74	6.14	5.68	8.57	1.16	11.92
SpX Dragon	9.64	4.30	3.98	6.61	8.11	8.35
Orbital Cygnus	20.11	8.98	8.31	12.54	16.92	17.43
PSLV	6.89	3.08	2.85	4.3	5.80	5.97

Launcher	(b) Monoblock Frame					
	Max. Total Deformation ($\times 10^{-6}$ m)			Max. von Mises Stress (MPa)		
	X	Y	Z	X	Y	Z
HTV	8.40	3.51	3.24	3.16	4.52	4.96
ATV	12.50	5.20	4.81	4.96	6.71	7.36
SpX Dragon	8.73	3.64	3.37	3.29	4.70	5.16
Orbital Cygnus	18.20	7.61	7.04	6.86	9.82	10.80
PSLV	6.24	2.61	2.41	2.35	3.36	3.69

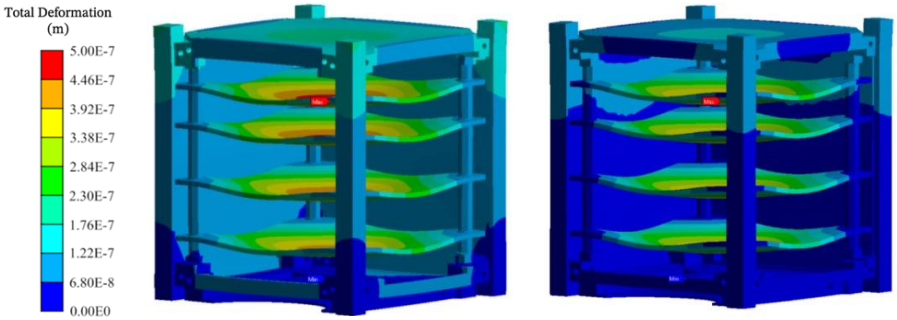

(a) (b)

Figure 12. Maximum total deformation during Orbital Cygnus launch on the X-axis: (a) Modular frame and (b) Monoblock frame

Regarding von Mises stress, the Orbital Cygnus launch vehicle produced the highest stress values, with a maximum of 17.43 MPa along the Z-axis for the modular frame and 10.80 MPa along the Z-axis for the monoblock frame. The lowest stresses were recorded with the PSLV launcher, at 4.30 MPa in the X-axis for the modular frame and 2.35 MPa in the X-axis for the monoblock frame. The stress concentrations were primarily observed at the recess feet of the satellite, which had to withstand harsh launch loads, as depicted in Figure 13. However, these stress levels remained significantly below the yield strength of Aluminium 6061, indicating that the structural integrity of these regions was maintained within acceptable limits.

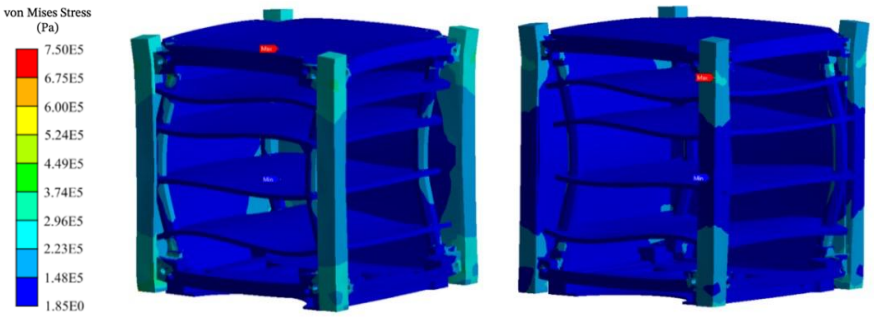

(a) (b)

Figure 13. Maximum von Mises stress results in Pa during Orbital Cygnus launch in the Z-axis: (a) Modular frame and (b) Monoblock frame

3.3 Modal Analysis

Table 12 lists the natural frequencies of the first six vibration modes of the modular and monoblock-frame designs. The difference between the first four modes for both frame designs was approximately 3.5 Hz. The monoblock frame design generally recorded a lower frequency value than the modular design. The computed first natural frequency mode is 679.99 Hz for the modular frame and 677.88 Hz for the monoblock frame. Figure 14 and Figure 15 shows the deformation patterns of the modular and monoblock frame designs caused by the first six vibration modes, respectively. The bending of the material of the first four modes primarily occurred on the satellite PCBs for both frame designs. However, deformation predominantly occurred at the standoffs in mode shapes 5 and 6 due to the nature of these higher-frequency oscillations. Higher vibration modes generally induce more complex deformation patterns transferred to structural points, such as standoffs. These standoffs, which function as nodes within the vibration pattern, experience localized stress concentrations. Furthermore, because standoffs serve as connection points between components (such as PCBs), they create leverage points where forces are amplified, resulting in greater displacements and deformations.

Table 12. Comparison of natural frequencies of modular and monoblock designs

Mode	Frequency (Hz)	
	Modular	Monoblock
1	679.99	677.88
2	684.34	682.68
3	687.35	686.44
4	688.62	671.68
5	971.15	998.03
6	1040.10	1046.90

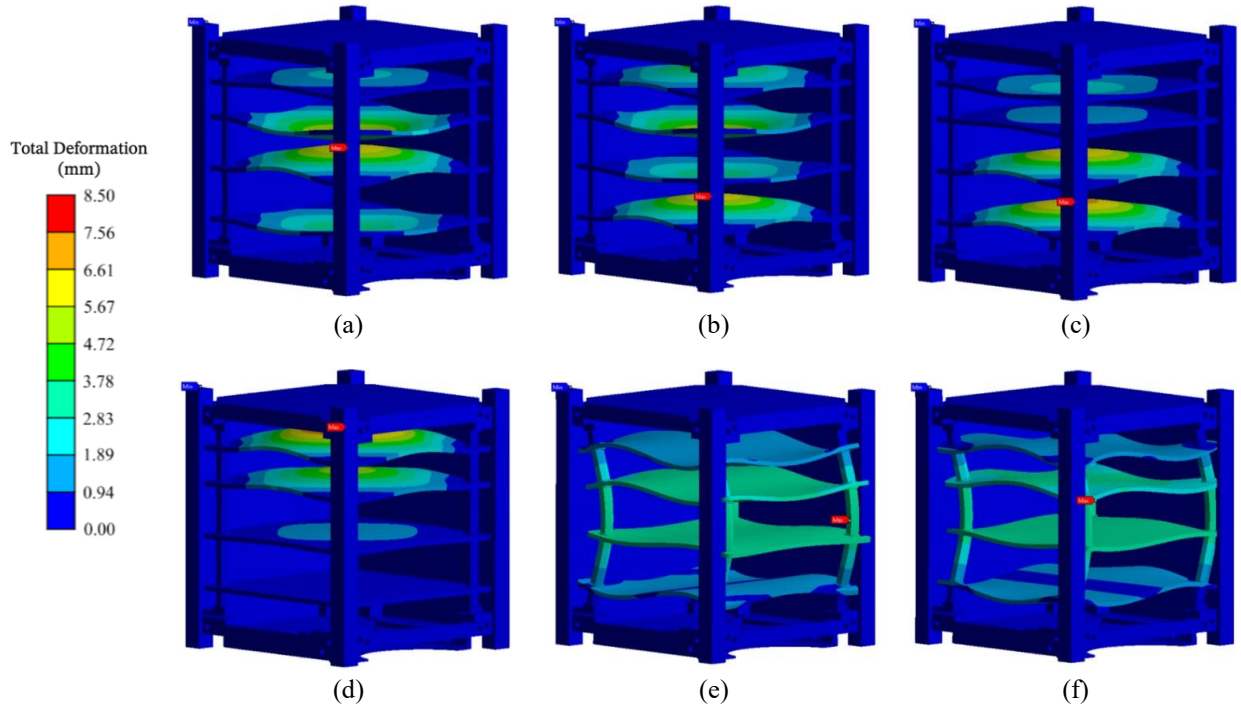

Figure 14. Mode shape results for the modular frame: (a) Mode 1, (b) Mode 2, (c) Mode 3, (d) Mode 4, (e) Mode 5, and (f) Mode 6

These values exceeded the minimum requirement, indicating that the frames met the specified criteria [27]. However, it is important to note that this analysis did not account for the presence of complete components within the satellite. Larger components, such as batteries, can significantly affect and potentially reduce the natural frequency. This finding aligns with those of [5] and [11], who stated that including larger components can substantially affect the natural frequency of a structure.

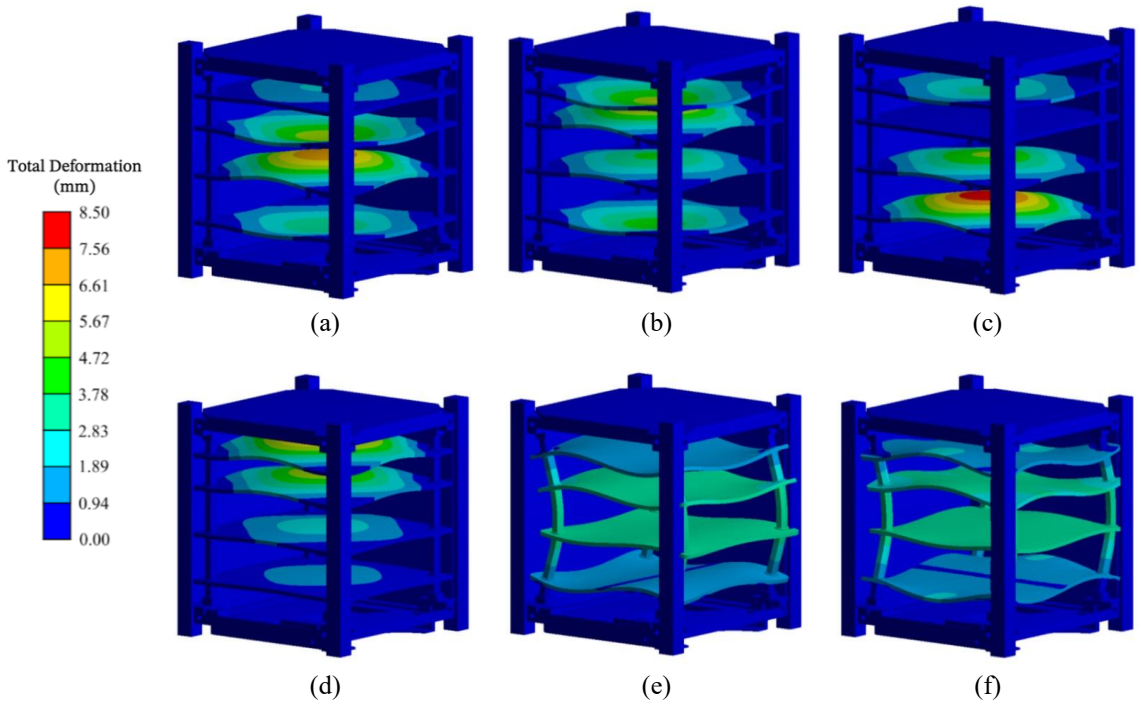

Figure 15. Mode shape results for the monoblock frame: (a) Mode 1, (b) Mode 2, (c) Mode 3, (d) Mode 4, (e) Mode 5, and (f) Mode 6

3.4 Random Vibration

Table 13 compares the maximum von Mises stresses from the random vibration analysis for the modular and monoblock frame designs across different launch vehicles. The results demonstrate notable variations in the stress levels between the two designs under different launch environments. This analysis recorded the highest stress when power spectral density data from PSLV were used. It should be clarified that the PSD data are derived from the launch vehicle and not from a manned deployment platform such as the HTV, ATV, SpaceX Dragon, or Orbital Cygnus, separated after several launch stages. It is important to note that the results of the random vibration analysis were statistically significant due to the random nature of the input loads.

For the modular frame, the highest von Mises stress was observed with the PSLV launcher, reaching 12.70 MPa, while the lowest stress was recorded with the SpaceX Dragon, producing 5.60 MPa. The Orbital Cygnus ATV HTV launch vehicles had moderate stress levels of 7.63, 8.19, and 7.25 MPa, respectively. The monoblock frame exhibited consistently higher von Mises stress values than the modular frame for all launch vehicles. The PSLV induced the greatest stress in the monoblock design, reaching 16.39 MPa, whereas the lowest stress occurred with the SpaceX Dragon, at 7.15 MPa. The Orbital Cygnus, ATV, and HTV launchers produced 9.74, 10.29, and 9.23 MPa stress levels, respectively.

Table 13. Comparison of the resulting maximum von Mises stress due to random vibration for both designs for different launch vehicles

Launcher	Max. von Mises Stress (MPa)	
	Modular	Monoblock
HTV	7.25	9.23
ATV	8.19	10.29
SpX Dragon	5.60	7.15
Orbital Cygnus	7.63	9.74
PSLV	12.70	16.39

The analysis revealed that most stresses were concentrated at the standoffs where all boards were placed, as shown in Figure 16. This phenomenon could potentially lead to loosening or damage to standoffs. These findings indicate that the monoblock frame generally experiences higher von Mises stress under random vibration than the modular frame across all launch vehicles. However, despite the higher stress values, the observed stress levels for both designs remained significantly lower than the yield strength of Al-6061. Therefore, based on the findings of [41], the effects of these stresses can be considered negligible. This suggests that both frame designs maintain structural integrity under random vibration loads encountered during the launch phase. The differences in stress levels between the two designs may be attributed to variations in the frame geometry and load distribution, with the monoblock frame potentially being more susceptible to random vibration forces.

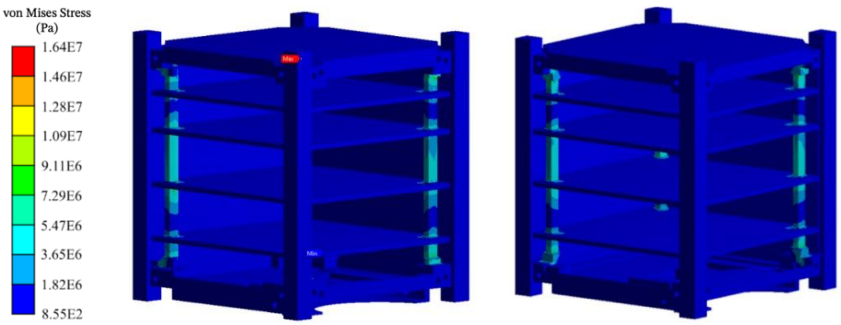

(a) (b)

Figure 16. von Mises stress results of MYSat structure under PSLV random vibration load: (a) modular and (b) monoblock

4. CONCLUSIONS

A comprehensive analysis of the modular and monoblock frame designs demonstrated their structural performance under various loading scenarios, including static and dynamic conditions. The static analysis revealed minimal deformations, ranging from approximately 1.6 to 4.4 × 10^{-7} m, and von Mises stress levels between 0.24 and 0.74 MPa. Notably, higher stresses and deformations were observed in Static Case 2 due to the larger applied load. The modular frame exhibited greater total deformation than the monoblock frame, which benefited from a unified structure that enhanced load distribution and resilience. The stress concentration resulting from design holes was also identified as a critical factor, underscoring the necessity for careful design considerations to mitigate potential failure risks. Under various launch conditions, the modular frame consistently demonstrated higher deformation and stress levels than the monoblock design. Specifically, the modular frame experienced maximum deformations of 20.11×10^{-6} m and peak von Mises stresses of 17.43 MPa under the Orbital Cygnus launcher. In contrast, the monoblock frame showed 18.20×10^{-6} m deformation and 10.80 MPa stress. Despite these elevated deformations, particularly at the top printed circuit boards, they were deemed negligible regarding the overall structural integrity. Stress concentrations were also identified at the recess feet; however, these values remained within the yield strength limits of Al-6061, ensuring the structural integrity of both frame designs.

The natural frequency analysis revealed that the monoblock frame generally exhibited lower natural frequency values, with the first recorded frequency at 677.88 Hz compared to 679.99 Hz for the modular frame. Deformation patterns were primarily observed on the printed circuit boards during the initial four vibrational modes, whereas higher modes led to significant deformations at the standoffs. This was attributed to the role of the standoffs as nodes within the vibration patterns, resulting in localized stress concentrations amplified because of their function as connection points between the various components. Random vibration analysis showed notable differences in the maximum von Mises stresses experienced by the modular and monoblock frame designs across various launch vehicles. Specifically, the modular frame recorded a peak stress of 12.70 MPa under the PSLV launch conditions, while the monoblock design reached a higher level of 16.39 MPa under the same conditions. Stresses were primarily concentrated at the standoffs that supported the circuit boards, indicating a potential risk of loosening or damaging these components.

Both frame designs demonstrated structural stability within the specifications for Aluminium 6061, confirming their ability to withstand the anticipated loads without exceeding the stress limits. Notably, both the designs met the minimum required natural frequency. Although the findings indicated that the monoblock frame exhibited enhanced structural resilience under launch conditions, it appeared more susceptible to random vibration forces. The differences in the stress response between the two designs can be attributed to the variations in their geometries and load distributions. Overall, the findings confirm the suitability of both frame designs for satellite applications, as they effectively withstand the applied loads while emphasizing the importance of design choice in optimizing structural integrity and performance. However, further evaluation in the context of full satellite integration is recommended to ensure a comprehensive performance assessment. In addition, the analysis did not account for larger satellite components, such as batteries, which could lower the natural frequency. This aligns with existing literature, suggesting that the inclusion of substantial components can significantly influence the structure's dynamic characteristics. Given the preliminary nature of the design, a detailed structural analysis of MYSat is advisable to obtain more information on the structural performance of the satellite. In addition, evaluating and comparing additional frame designs would assist in enhancing the current design and achieving a structurally optimized MYSat frame. Experimental verification and validation are essential to assess the final structural design.

ACKNOWLEDGEMENTS

The authors acknowledge the computational facilities provided by the CAD Lab, School of Aerospace Engineering, Universiti Sains, Malaysia. The authors also thank Enago (www.enago.com) for the English language review. This research was financially supported by the Research Universiti Sains Malaysia Grant (1001/PAERO/8014005).

CONFLICT OF INTEREST

The authors declare that they have no known competing financial interests or personal relationships that could influence the work reported in this study.

AUTHORS CONTRIBUTION

A. S. Mohamed Thaheer (Writing - original draft; Methodology; Software; Formal analysis)

N. A. Ismail (Writing - review & editing; Conceptualization; Funding Acquisition; Supervision)

M. H. H. Amir (Software; Formal analysis)

N. Abdul Razak (Writing - review & editing; Validation)

AVAILABILITY OF DATA AND MATERIALS

The data supporting this study's findings are available on request from the corresponding author.

ETHICS STATEMENT

Not applicable.

REFERENCES

[1] M. Swartout, "The first one hundred CubeSats: A statistical look," *Journal of Small Satellite*, vol. 2, no. 2, pp. 213–233, 2013.

[2] A. S. M. Thaheer, N. A. Ismail, S. H. Md. Yusoff, Mohd. I. Yamin, N. A. Razak, "Mission analysis and design of MYSat: A 1U Cubesat for electron-density measurement," in *68th Astronautical Congress,* Adelaide, Australia, 2017.

[3] A. S. M. Thaheer, N. A. Ismail, "Orbit design and lifetime analysis of MYSat: A 1U CubeSat for electron-density measurement," in *4th NatGrad Conference*, Selangor, Malaysia, 2017.

[4] K. Cote, J. Gabriel, B. Patel, N. Ridley, Z. Taillefer, S. Tetreault, "Mechanical, power, and propulsion subsystem design for a CubeSat," *Technical Report*, Worcester Polytechnic Institute, 2011.

[5] S. Raviprasad, N. S. Nayak, "Dynamic analysis and verification of structurally optimized nano-satellite systems," *Journal of Aerospace Science and Technology*, vol. 1, no. 2, pp. 78-90, 2015.

[6] G. I. Barsoum, H. H. Ibrahim, M. A. Fawzy, "Static and random vibration analyses of a university CubeSat project," *Journal of Physics: Conference Series*, vol. 1264, no. 1, p. 012019, 2019.

[7] S. S. Isharuddin, M. Okasha, S. Ibrahim, "IIUM CubeSat structural subsystem design," *Advanced Materials Research*, vol. 1115, pp. 568–572, 2015.

[8] H.-U. Oh, S.-H. Jeon, S.-C. Kwon, "Structural design and analysis of 1U standardized STEP Cube lab for on-orbit verification of fundamental space technologies," *International Journal of Materials, Mechanics and Manufacturing*, vol. 2, no. 3, pp. 239–244, 2014.

[9] K. Sekerere, T. Mushiri, "Finite element analysis of a Cubesat," in *International Conference on Industrial Engineering and Operations Management (IEOM2017)*, Bristol, United Kingdom, 2017.

[10] A. Alhammadi, M. Al-Shaibah, A. Almesmari, T. Vu, A. Tsoupos, F. Jarrar, et al., "Quasi-static and dynamic response of a nano-satellite during launching," in *Proceedings of the 8th European Conference for Aeronautics and Space Sciences*, pp. 1-10, 2019.

[11] A. Ampatzoglou, A. Baltopoulos, A. Kotzakolios, V. Kostopoulos, "Qualification of composite structure for Cubesat picosatellites as a demonstration for small satellite elements," *International Journal of Aeronautical Science & Aerospace Research*, vol. 1, no. 1, pp. 1–10, 2014.

[12] A. Ampatzoglou, S. Tsantzalis, D. E. Mazarakos, V. Kostopoulos, "3D printed frame for CubeSat applications for low-earth orbit mission," *International Journal of Computer Aided Engineering and Technology*, vol. 9, no. 4, pp. 434-452, 2017.

[13] J. E. H. Arroyave, J. A. Ferrer-Pérez, A. Colin, B. Bermúdez-Reyes, "CubeSat system structural design," in *67th International Astronautical Congress*, Guadalajara, Mexico, pp. 1-5, 2016.

[14] E. E. Bürger, G. Loureiro, R. Z. G. Bohrer, L. L. Costa, "Development and analysis of a Brazilian Cubesat structure," in *22nd International Congress of Mechanical Engineering (COBEM 2013)*, Rebeirao Preto, Brazil, pp. 1-10, 2013.

[15] G. Capovilla, E. Cestino, L. M. Reyneri, G. Romeo, "Modular multifunctional composite structure for CubeSat applications: Preliminary design and structural analysis," *Aerospace*, vol. 7, no. 2, p. 17, 2020.

[16] M. Cihan, A. Cetin, M. O. Kaya, G. Inalhan, "Design and analysis of an innovative modular cubesat structure for ITU-pSAT II," in *Proceedings of 5th International Conference on Recent Advances in Space Technologies,* Istanbul, Turkey, pp. 494–499, 2011.

[17] R. De La Vega-Ibarra, B. Romero-Ángeles, D. Torres-Franco, A. Molina-Ballinas, L. A. De La Vega-Ibarra, "Análisis de resistencia estructural en el diseño de un nanosatélite CubeSat," *Científica*, vol. 23, no. 2, pp. 141–148, 2019.

[18] A. Dhariwal, N. Singh, A. K. Kushwaha, "Structural analysis of 1U CubeSat designed for low earth orbit missions," in *2023 International Conference on IoT, Communication and Automation Technology (ICICAT)*, Gorakhpur, India, pp. 1–5, 2023.

[19] C. Quiroz-Garfias, G. Silva-Navarro, H. Rodriguez-Cortes, "Finite element analysis and design of a CubeSat class picosatellite structure," in *4th International Conference on Electrical and Electronics Engineering*, Mexico City, Mexico, pp. 294–297, 2007.

[20] S. Waydo, D. Henry, M. Campbell, "CubeSat design for LEO-based earth science missions," in *IEEE Aerospace Conference*, Montana, United States, pp. 435-445, 2002.

[21] N. Athirah, M. Afendi, K. Hafizan, N. A. M. Amin, M. S. A. Majid, "Stress and thermal analysis of CubeSat structure," *Applied Mechanics and Materials*, vol. 554, pp. 426–430, 2014.

[22] M. Parab, A. Sapre, P. Pesode, P. Dhatrak, "Optimization of 1U nanosatellite on the basis of strength and weight using different Materials: A numerical approach," *Materials Today: Proceedings*, vol. 62, pp. 4073–4080, 2022.

[23] F. T. Al-Maliky, M. J. AlBermani, "Structural analysis of Kufasat using Ansys program," *Artificial Satellites*, vol. 53, no. 1, pp. 29–35, 2018.

[24] R. Sandau, H.-P. Roeser, A. Valenzuela. Small Satellite Missions for Earth Observation. 1st Ed. Berlin: Springer Berlin Heidelberg, 2010.

[25] H. R. Chiranjeeve, K. Kalaichelvan, A. Rajadurai, "Design and vibration analysis of a 2U-CubeSat structure using AA-6061 for AUNSAT-II," *IOSR Journal of Mechanical and Civil Engineering*, vol. 1, pp. 61–68, 2014.

[26] G. Miglioreno, T. K. Henriksen. The International Handbook of Space Technology. 1st Eds. Berlin, Heidelberg: Springer Berlin Heidelberg, 2014.

[27] JAXA, "Small Satellite Deployment Interface Control Document," *JEM Payload Accommodation Handbook*, JX-ESPC-101133-D, 2020.

[28] ISIS, "CubeSat Structures," Technical Brochure, Innovation Solution in Space [Online], 2017. Available: https://www.isispace.nl/

[29] M. Garg, J. Sembera, M. Franki, "CubeSat Final Report," University of Texas, Austin, Texas, USA, 2003.

[30] A. Israr, "Vibration and modal analysis of low earth orbit satellite," *Shock and Vibration*, vol. 2014, pp. 1–8, 2014

[31] A. C. Okolie, S. O. Onuh, Y. T. Olatunbosun, M. S. Abolarin, "Design optimization of Pico-satellite frame for computational analysis and simulation," *American Journal of Mechanical and Industrial Engineering*, vol. 1, no. 3, pp. 74–84, 2016.

[32] K. Nakaya, K. Konoue, H. Sawada, K. Ui, H. Okada, N. Miyashita, et al., "Tokyo Tech CubeSat: CUTE-I - Design & development of flight model and future plan," in *21st International Communications Satellite Systems Conference and Exhibit*, Yokohama, Japan, 2003.

[33] A. Ampatzoglou, V. Kostopoulos, "Design, analysis, optimization, manufacturing, and testing of a 2U Cubesat," *International Journal of Aerospace Engineering*, vol. 2018, pp. 1–15, 2018.

[34] ASM International. Properties and Selection: Nonferrous Alloys and Special-Purpose Materials, 10th Eds. Ohio, United States: ASM International, 1992.

[35] J. R. Davis. ASM Specialty Handbook: Stainless Steel. 1st Ed. Ohio, United States: ASM International, 1994.

[36] J. R. Davis. ASM Specialty Handbook: Copper and Copper Alloys. 1st Ed. Ohio, United States: ASM International, 2001.

[37] M. Bertha, "OUFTI-1 nanosatellite: Dynamic analysis and qualification testing," *Master Thesis*, University of Liège, Liège, Belgium, 2010.

[38] D. Geeroms, S. Bertho, M. De Roeve, R. Lempens, M. Ordies, J. Prooth, "ARDUSAT, An Arduino-based CubeSat providing students with the opportunity to create their own satellite experiment and collect real-world space data," in *22nd ESA Symposium on European Rocket and Ballon Programmes and Related Research*, Norway, pp. 643-648, 2015.

[39] A. L. Hill, "NPS-SCAT CONOPS and radiation environment," *Master Thesis*, Naval Postgraduate School, California, United States, 2012.

[40] J. R. Wertz, D. F. Everett, J. J. Puschell. Space mission engineering: The new SMAD. 1st Ed. Hawthorne, Ohio, United States: Microcosm Press, 2011.

[41] Y. Nogawa, S. Imai. Launch from the ISS, in Cubesat Handbook: From Mission Design to Operations. 1st Ed. United States: Academic Press, 2020.

[42] C. Kilic, A. R. Aslan, "Mission analysis of a 2U CubeSat, BeEagleSat," in *7th International Conference on Recent Advances in Space Technologies (RAST)*, Istanbul, Turkey, pp. 835–838, 2015.

[43] J. Blazek. *Computational Fluid Dynamics: Principles and Applications*, 3rd Eds. United Kingdom: Butterworth-Heinemann, 2015.

[44] T. S. Mahesh Babu, V. George Koshy, D. Bharath, "Thermal and vibrational analysis of Cubesat," *Applied Mechanics and Materials*, vol. 766–767, pp. 1091–1096, 2015.

[45] R. G. Budynas, J. K. Nisbett. *Shigley's Mechanical Engineering Design*. 10th Eds. New York: McGraw-Hill Education, 2015.

[46] NASA, "General Environmental Verification Standard (GEVS) for GSFC Flight Programs and Projects," *Goddard Technical Standard*, GSFC-STD-7000B, 2021.

[47] JAXA, "Small satellite deployment interface control document," *JEM Payload Accommodation Handbook*, vol. 8, JX-ESPC-101133-B, 2013.

[48] S. Ramakrishnan, S. V. Sharma, L. Sowmianarayanana, "Small satellite launch opportunities on PSLV," in *Euro-Asia Space Week on Cooperation in Space*, vol. 430, pp. 547-556, 1999.

[49] G. F. Abdelal, N. Abuelfoutouh, A. H. Gad, *Finite Element Analysis for Satellite Structures: Applications to Their Design, Manufacture and Testing*. 1st Ed. London: Springer, 2013.

[50] R. C. Hibbeler. Mechanics of Materials. 10th Eds. Boston: Pearson, 2017.

[51] ANSYS, "ANSYS mechanical APDL structural analysis guide," *ANSYS Inc*., 2013.